Crustal Magnetization of Mars: Terra Meridiani and Terra Sirenum

Renee A. French, Donna M. Jurdy*

Department of Earth and Planetary Sciences, Northwestern University, Evanston, IL, USA
Email: *donna@earth.northwestern.edu

Abstract

We examine the crustal magnetization of Terra Meridiani and Terra Sirenum, the region representing the strongest magnetization in the Southern Hemisphere, by downward continuing mapping level data (400 km altitude) from the Mars Global Surveyor (MGS) Magnetometer and Electron Reflectometer (MAG/ER). We find that the surface magnetization in both regions can be fit with a small number of sources, with the positive sources stronger than negative ones in both regions. The ratio of the strongest positive to strongest negative source for the regions matches within 2%. For both regions, the locations of strong sources are positioned at the outer rings of ancient impact features. We employ two approaches of source depth estimation. One method employs downward continuation of positive and negative sources from mapping level into the subsurface to extrapolate the depth to magnetization. With this approach, source depths generally range from 80 ± 20 km in Terra Meridiani and 65 ± 25 km in Terra Sirenum. A graphical approach uses the contour map of surface magnetization to estimate depths ranging from 125 km for thick sources in Terra Meridiani and from 82 km for thick sources in Terra Sirenum. These depths require a low ($\leq{\sim}20$ mW/m^2) Martian heat flux to permit magnetite, hematite, and/or pyrrhotite (although limited) as carriers through 100 km or more. The upcoming InSight mission will provide invaluable seismic constraints on both crustal and core structure, in addition to the first Martian heat flow measurements that will constrain magnetization.

Keywords

Mars, Crustal Magnetization, Magnetization Depth,
InSight Mission, Geophysics

1. Introduction

Mars, with a radius of 3394 km, measures only about the size of Earth's core.

This small size means that it cooled faster than larger terrestrial planets and has experienced a decline in geologic activity, as observed by its relatively old surface. Faster cooling also limits the duration of a liquid core and potential global dynamo. Indeed, it was not suspected that Mars possessed a global core dynamo early in its history until the arrival of the Mars Global Surveyor (MGS) mission. Numerous orbiters and landers have surveyed Mars, with data for crustal magnetization collected by MGS. Prior to entering a circular, polar orbit at ~400 km altitude ("mapping" phase), MGS was placed into a highly elliptical orbit ("aerobraking" phase) and the Magnetometer and Electron Reflectometer (MAG/ER) collected data from 80 - 190 km altitude [1] [2]. Although the MAG/ER measurements at aerobraking altitudes are spatially discontinuous, they revealed a strongly magnetized crust (up to ~1600 nT at 100 km altitude) over large portions of the surface even though Mars does not currently possess a magnetic field. More continuous mapping-level measurements by MGS followed this discovery.

The magnitude of remanent crustal magnetization provides unambiguous evidence that Mars once had a global core dynamo [1] [3]. Timing constraints for an active core dynamo are based on thermal and impact demagnetization [4] [5] [6] [7] and the paleomagnetic record of meteorite ALH84001 [8] [9], placing activity as late as ~4 Ga. The reason for core dynamo shut off remains largely unknown, with hypotheses ranging from rapid cooling, complete core freezing [10] to convection disruption by large impacts [11]. Since crustal magnetization predates many old impact basins, it dates as one of the oldest features of Mars and points to activity early in its history. However, some large impact basins have modified the strength of crustal magnetization either through impact demagnetization of pre-existing magnetized crust or remagnetization (crust that was shock-heated above the Curie temperature) in the presence of a core dynamo [12]. Indeed, the location of certain magnetic sources was shown to associate with outer rings of large impact basins in the strongly magnetized region of the Southern Hemisphere (centered on 40˚S, 180˚) [13]. The age of these impact basins constrains the timing of the core dynamo.

In this study, we examine remanent magnetization in Terra Meridiani. We undertake a comparable analysis for Terra Sirenum (termed here for brevity as the region that represents the strongest magnetization in the Southern Hemisphere) for comparison of field properties to Terra Meridiani. We then select the strongest anomalies as possible magnetic sources for both regions and use two different approaches to estimate the depth of magnetization.

2. Background

2.1. Terra Meridiani

Terra Meridiani spans a region near 0˚N, 0˚E, east of Tharsis and Valles Marineris. Terra Meridiani is part of the Noachian-aged heavily cratered terrain [14] [15] [16] and was the target of the Mars Exploration Rover (MER) Opportunity mission, partly to explore the largest surficial deposit of hematite on the planet

[17]. MER Opportunity analyzed a section of rock known as the Burns Formation, which revealed past arid, acidic, and oxidizing environments influenced by a fluctuating groundwater table [18] [19] [20] that probably occurred no later than the Hesperian [21].

Terra Meridiani encompasses a significant crustal magnetic signature [1] and has been the site of two proposed "great faults" [3] [22]. Fault locations are approximated based on offsets of the magnetic field at 400 km altitude that remain as the data is downward continued, as well as the magnitude of alternating polarity across the offsets. Thus, these are interpreted as transform faults along which divergent plate boundaries were situated, suggesting that Terra Meridiani was once the site of an active plate boundary [3]. Earlier, it was speculated that this region could have hosted early Martian plate tectonics, but with a subduction zone for a northern hemisphere oceanic-type plate [23].

2.2. Terra Sirenum

For brevity in this paper, we use Terra Sirenum for the area encompassing the Terra Sirenum and Terra Cimmeria regions in the southern hemisphere of Mars. The area is centered at roughly 40°S, 180° and spans ±30° latitude and ±60° longitude, with Terra Cimmeria located in the western portion and Terra Sirenum to the east. This heavily cratered region represents Noachian aged terrain, with some localized geologic units forming in the early Hesperian [14] [15] [16]. East-west trending magnetic lineations in this region were first detected by the magnetometer on MGS and have been modeled as shallow, large-scale dikes possibly associated with an early episode of seafloor-type spreading [24] [25].

Magnetization in this region was analyzed [13] [26] in order to clarify the nature and timing of the most continuous, expansive, and intense magnetization on Mars. Data from mapping altitude (400 km) was downward continued and found to have a 95% correlation with the vertical component of anomalies in both the downward continued and aerobraking data at 100 km altitude [26]. Since the low level data did not reveal any magnetic features not represented in the mapping data, it was concluded that magnetic sources must have wavelengths ≥400 km. A deconvolution was used to model 10 - 12 discrete sources (more positive than negative) with depths ≥100 km that could represent the field in Terra Sirenum. This model also confirmed the association between some magnetic anomalies and the outer rings of large impact basins by performing a chi-squared analysis. Positive sources in this region outnumber negative ones, exceed them in amplitude, and display different downward continuation, hinting at fundamental differences in polarity properties of Mars' ancient magnetic field [13].

2.3. Existing Estimates of Magnetization and Magnetic Layer Thickness/Depth

Previous workers have utilized a number of different methods for estimating average global magnetization and magnetic depth of the Martian crust. One study

[27] inverted radial magnetic field observations and fit them to a mesh of 11,550 equally spaced, radially oriented dipoles to obtain a source of magnetization distribution. By assuming the average crustal thickness of 50 km [28] for the solution, a maximum magnetization of −22 A/m for negative sources and 17 A/m for positive sources was obtained. Analysis of impact demagnetization around large craters [29] gives an estimation of a magnetic depth, if uniform, of ~35 km with a range of 10 - 100 km. Furthermore, these depths, combined with the observed magnetic anomalies, suggest magnetizations of 5 - 40 A/m. Another study [30] analyzed Mars' magnetic spectrum and fit it to a theoretically derived power spectrum assuming random magnetic sources. Only a crustal field was found (unlike a crust and core field for Earth), about 46 km thick, with a magnetization about 9.6 ± 3.2 times stronger than Earth's. A mathematical investigation [31], without assumptions regarding magnetization direction, concluded that if magnetization was confined to a 50 km thick layer, the minimum intensity is at least 4.76 A/m for a three-dimensional model, 6.038 A/m for a two-dimensional model, and 5.132 A/m for a model using a single observed Bz value. One study [32] performed an inversion of all three components of the magnetic field data, which was used to generate an equivalent source representation, to predict magnetic measurements in a least-squares fit. By assuming the magnetization was confined to a 40 km thick layer (consistent with previous studies), the magnetization ranges between ±12 A/m. Additionally, a model made for the thermal evolution of Mars [33] used parameterized convection calculations to determine magnetic layer thickness for each potential mineral source. These models predicted thicknesses at ~4 Ga that range from ~30 - 130 km for hematite, ~25 - 120 km for magnetite, and ~20 - 70 km for pyrrhotite.

Other studies have focused efforts on regional estimates of magnetization and magnetic depth. Magnetization of the Terra Cimmeria region was estimated by assuming source dimensions based on MGS data [24]. Best-fit models of multiple quasi-parallel linear features that are ≥ 200 km wide, 2000 km long, and 30 km thick yield a volume magnetization of −20 A/m for negative sources and 20 A/m for positive sources. Similarly, a model [25] was made for the same region using 200 km wide, 2000 km long dikes that are 5 km below the surface. An estimation of a 35 - 60 km thick prism with a magnetization of 15 A/m could reproduce the observed magnetic anomaly amplitude of 1000 nT. An investigation of the Apollinaris Patera magnetic anomaly with iterative forward modeling of one or more uniformly magnetized circular disks was used to determine the magnetic source [34]. However, based on assumptions made such as Martian core dynamo strength and Curie point isotherms for hematite, magnetite, and pyrrhotite [33], and an assumed maximum source thickness of 3 km, a minimum magnetization of 50 A/m was deduced [34].

2.4. Magnetic Minerals

Thermoremanent magnetization (TRM) that has been stable over billions of years offers the most likely cause of the Martian magnetic anomalies. This happens

when a mineral cools through its Curie temperature, *i.e.*, the temperature below which a mineral captures the magnetization of an external field. Only iron oxide and iron sulfide minerals can retain considerable remanent magnetization over geologically long periods of time. A recent study [33] selected terrestrial magnetic minerals (*i.e.*, magnetite, titanomagnetite, hematite, titanohematite, and pyrrhotite) as potential Martian magnetic minerals were selected for thermal evolution models. Martian meteorites have been found to contain such minerals, like magnetite, titanomagnetite, and pyrrhotite [8] [35]. Magnetite, titanomagnetite, pyrrhotite, and hematite have been determined as effective TRM carriers for the Martian crust and that a 30 km thick sheet containing <2% multi-domain (grain diameter ≥15 μm) hematite could explain the observed magnetic anomalies [36]. Interestingly, the Thermal Emission Spectrometer (TES) on the MGS detected a surface deposit of coarse (>10 μm) crystalline hematite in Terra Meridiani [37]. This hematite, in the form of spherules or "blueberries", likely formed diagenetically as a fluctuating groundwater table in the late Noachian interacted with olivine-rich basalt sands [19] [38] [39].

The Rock Abrasion Tool (RAT) on Mars Exploration Rovers (MERs) Spirit and Opportunity was used to determine the magnetization of target rocks in Gusev crater and Terra Meridiani, respectively. These measurements provide constraints on which magnetic minerals could be a source of observed regional magnetization. Fresh surfaces exposed by RAT and data from mineral identification instruments indicate that hematite and magnetite, or an oxidized variety of magnetite, are prime candidates for magnetic minerals [40].

The depth to which magnetic minerals retain magnetization depends largely (although not solely) on the Martian heat flux. However, the heat flux during the active Martian core dynamo remains unknown; numerous studies have generated a broad range of estimates. One method of estimating Martian heat flux includes convective thermal evolution models that incorporate heat from core segregation, radioactive element (U, Th, K) abundance, and crustal thickness variation [41] [42] [43]. These models produce a wide range of heat flux estimates, from 2 - 100 mW/m^2 at 4.0 Ga to 300 mW/m^2 at 4.5 Ga. Estimates of the depth to the base of the magnetized layer from impact demagnetization determined a 4.0 Ga heat flux of 53 - 67 mW/m^2 [29]. Combined gravity and topography data was used to estimate the thickness of the elastic lithosphere, which can then be used to estimate heat flux [28] [44]. Models produce a heat flux range of 37 - 57 mW/m^2 for an "early" Mars [28] and 20 - 60+ mW/m^2 before 3.7 Ga [44]. Models for Martian thrust faults estimate the seismogenic layer thickness at the time of faulting (~3.7 - 4.0 Ga), resulting in heat flux estimates ranging from 17 - 32 mW/m^2 with the actual value likely closer to the lower bound [45]. Table 1 lists possible magnetic carriers, their Curie temperatures [46], and magnetized depth estimates for various heat fluxes ranging from 3.7 - 4.5 Ga. The magnetized depth is calculated using $(T_c - T_s)k/F$ where k is thermal conductivity (3 W/(m·K)), T_c is Curie temperature (K), T_s is surface temperature (assumed to be 230 K [33]) and F is heat flux (W/m^2). The wide range of heat flux estimates yields a wide range of possible magnetized depths for each magnetic mineral.

Table 1. Possible magnetic minerals of the Martian crust, their Curie temperatures [46], and the depth at which their Curie temperature is reached for multiple estimates of Martian heat flux ~3.7 - 4.5 Ga. Magnetic minerals are considered end members if part of a series (e.g., magnetite-titanomagnetite). The magnetized depth is calculated using $(Tc - Ts)k/F$, where k is thermal conductivity (3 W/(m·K)), Tc is Curie temperature (K), Ts is surface temperature (assumed to be 230 K [33]), and F is heat flux (W/m^2).

Likely Magnetic Minerals	Curie Temp (K)	Magnetized depth 1a (km)	Magnetized depth 2b (km)	Magnetized depth 3c (km)	Magnetized depth 4d (km)	Magnetized depth 5e (km)	Magnetized depth 6f (km)	Magnetized depth 7g (km)
titanomagnetite	123	-	-	-	-	-	-	-
magnetite	853	6.2	18.7 - 934.5	27.9 - 35.3	28.3	58.4 - 109.9	37.4 - 93.5	32.8 - 50.5
titanohematite	73	-	-	-	-	-	-	-
hematite	953	7.2	21.7 - 1084.5	32.4 - 40.9	32.9	67.8 - 127.6	43.4 - 108.5	38.1 - 58.6
pyrrhotite	598	3.7	11 - 552	16.5 - 20.8	16.7	34.5 - 64.9	22.1 - 55.2	19.4 - 29.8

a Using a 4.5 Ga heat flux of 300 mW/m^2 [42]. b Using a 4 Ga heat flux range of ~2 - 100 mW/m^2 [41]. c Using a 4 Ga heat flux range of 53 - 67 mW/m^2 [29]. d Using a 4 Ga heat flux of 66 mW/m^2 [22]. e Using a 4.0 - 3.7 Ga global mean heat flux range of 17 - 32 mW/m^2 [45], with the true value likely closer to the lower heat flux bound. f Using a >3.7 Ga heat flux range of 20 - 50+ mW/m^2 [44]. g Using an "early" Mars heat flux range of 37 - 57 mW/m^2 for Terra Cimmeria, Arabia Terra, and Noachis Terra [28].

3. Methods

Magnetization maps of the Terra Meridiani and Terra Sirenum regions were created using MGS Magnetometer mapping level data from ~400 km altitude. We consider only the vertical component (Bz) of the magnetic field in our downward continued maps because it better represents the surface magnetization, as solar wind interferes more strongly with the horizontal (Bx and By) components [47]. For Terra Meridiani, we consider the subset of data within 20° latitude and longitude of 0°, smaller than the one used for our Terra Sirenum analysis (40°S ± 40°, 180°W ± 40°). Employing the approach of Cartesian transformation [13] [26], we rotated the coordinate system so that it was centered in each region and converted the spherical coordinates of the magnetic data to Cartesian coordinates. Although the approximation of spherical variables φ, θ, and r as Cartesian variables x, y, and z may seem coarse, for our rotated coordinate system it results in 0% error at the center, ~2% error at 20° from center, and ~8.5% error at 40° from center for Terra Sirenum [13] and the errors would be even less at the boundaries for Terra Meridiani (due to its location at the equator and smaller study area).

Using these Cartesian coordinates, we apply an ordinary two-dimensional Fourier transform analysis for downward continuation, which transforms the original magnetic signal (approximated as a Fourier sine series) into the frequency domain and is then multiplied by the continuation function $e + k\Delta z$ where k is wavenumber and z is distance [48]. Since downward continuation amplifies the source (signal *and* noise), wavenumbers $k \geq 25$ are dropped to minimize contribution from noise. It has also been shown that, when using Cartesian coordinates, the components of the original magnetic field agree very well with the gradient components of the derived scalar potential. Technical details and the validity of the transformation, for Terra Sirenum region, have been given in detail [13] [26].

We chose to display MGS aerobraking data at 110 km for Terra Meridiani and 100 km for Terra Sirenum because those respective altitudes contain the most continuous aerobraking data for these two regions. Outer rings of large impact basins for Terra Meridiani and Terra Sirenum are from published compilations [49] [50]. For our analysis, the locations of possible magnetic sources for both regions were visually selected at the sites of contour highs and lows (*i.e.*, the positions of "Bull's Eyes") on the generated surface maps and then numbered in order of strength: 1 - 5 for positive sources (those with the equivalent dipole directed outward) and 1' - 5' for negative sources in Terra Meridiani, and 1 - 7 for positive sources and 1' - 7' for negative sources in Terra Sirenum.

4. Results

Mapping data from 400 km altitude (Figure 1(A)) was downward continued to 110 km and correlated with raw aerobraking data at the same altitude (Figure 1(B)). While a majority of the signatures could be correlated and the magnitudes of the negative anomalies generally agree, the magnitudes of the downward continued positive anomalies are higher than those of the aerobraking data. Maximum and minimum B_z values for downward continued data at this altitude are 138 and −91 nT, while those for the aerobraking data are 278 and −268 nT. Downward continued magnetization of the surface is shown in Figure 1(C), where numbers 1 - 5 correspond to possible positive sources and 1'-5' to possible negative sources (see Section 5.1). Source 5 overlaps with the largest surficial deposit of hematite. Areas of strongest magnetization in the raw data, −27.55 nT (11.5°S, 1.5°E) and 31.07 nT (1.5°N, 343.5°E), correlate with areas of strong magnetization at 110 km altitude and at the surface.

Strong anomalies often correlate with outer rings of large multi-ring basins, the diameters and locations of which have been mapped [49] [50]. Figure 1(D) shows an expanded region, 35° × 35°, to give context to the relevant basins in the 20° × 20° maps in Figures 1(A)-(C). The strongest anomaly is located in the western portion of the map, overlapped by the outer two rings of the Chryse basin (formed between 4.1 - 4.2 Ga [51]) and Aram Chaos. The outer two rings of Chryse also overlap the second strongest positive anomaly and the strongest negative anomaly. The fourth strongest positive anomaly lies along the outer ring of the basin labeled "overlapped by Newcomb". However, no anomalies of significant strength seem to be adjacent to the "overlapped by Schaparelli" basin.

4.1. Terra Sirenum

Figure 2 shows crustal magnetization maps for Terra Sirenum. Data from 400 km altitude (mapping data, Figure 2(A)) is downward continued to 100 km for comparison with aerobraking data at corresponding altitude (Figure 2(B)). The location and relative magnitude of downward continued magnetic anomalies agree with anomalies in the aerobraking data. The area of strongest positive magnetization in the mapping data, 175 nT (51°S, 179°E), corresponds with the strongest anomalies at 100 km and at the surface (Figure 2(C)). In Figure 2(C),
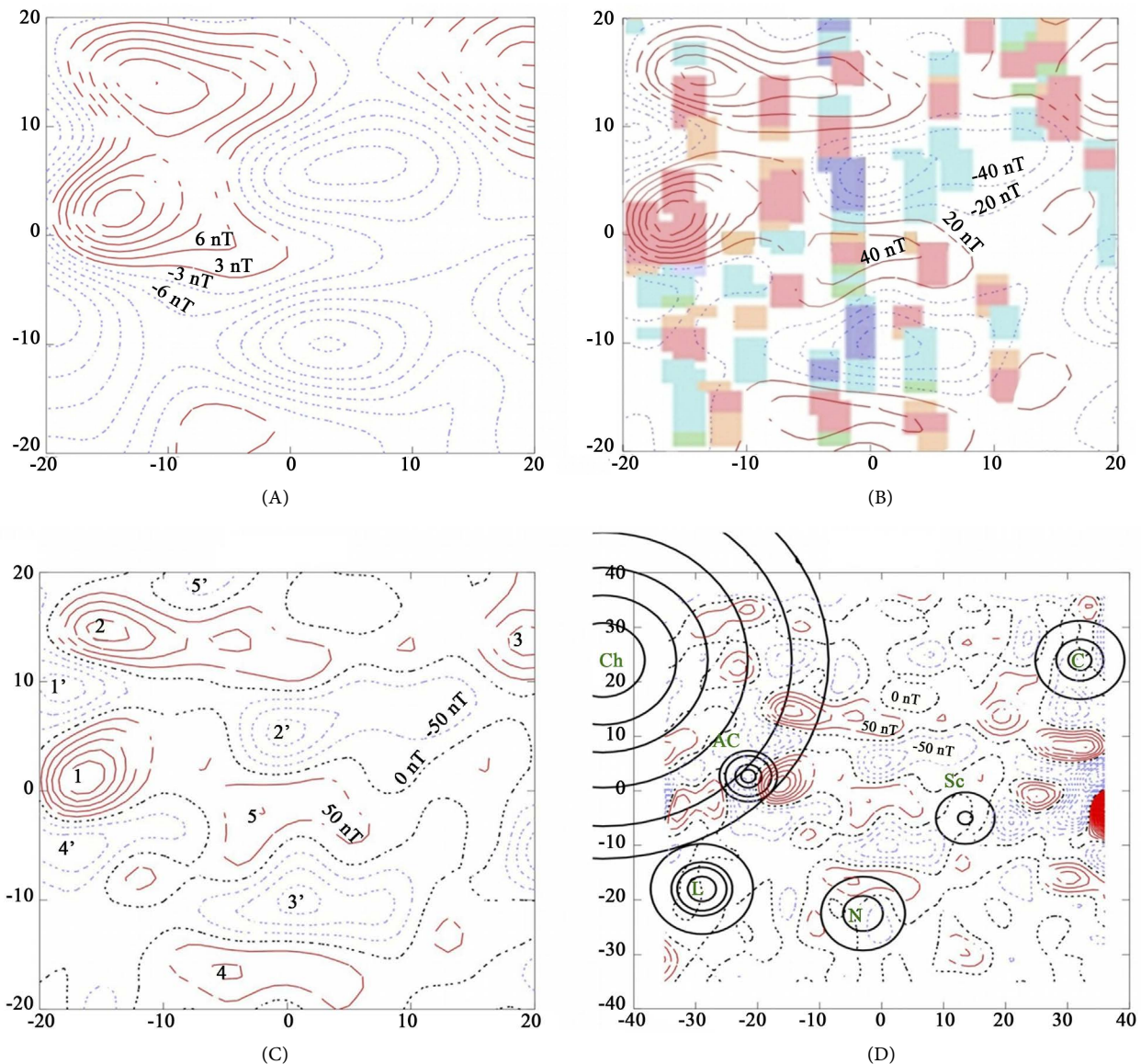
Figure 1. Magnetization in Terra Meridiani. Each base map uses MGS MAG Br data, where red contours represent positive anomalies and blue contours represent negative anomalies (black lines are 0 nT). (A) Data collected at 400 km (mapping) altitude (contour interval of 3 nT); (B) 400 km data downward continued to 110 km (contour interval of 20 nT) and correlated with aerobraking data (swaths) collected at the same altitude. In the swaths, red represents Br > 150 nT, orange is 150 > Br > 50, green represents −50 < Br < −150, light blue represents −150 < Br < −250, and dark blue represents Br < −250 nT; (C) 400 km data downward continued to the surface (contour interval is 50 nT). The numbers correspond to possible sources of magnetization; (D) Surface magnetization (contour interval is 50 nT) expanded to ~35° × 35° with regional multi-ringed basins [49] (Ch = Chryse, L = Ladon, AC = Aram Chaos, N = overlapped by Newcomb, Sc = overlapped by Schiaparelli, C = Cassini).

numbers 1 - 7 correspond to possible positive sources and 1'-7' to possible negative sources (see Section 5.1).

Magnetic anomalies of significant strength are associated with outer rings of large impact basins (**Figure 2(D)**), with statistical detail given in a previous study [13]. In particular, the outer ring of the Sirenum basin (formed between 4.1 - 4.2 Ga [51]) coincides with the three strongest positive anomalies and the sixth strongest negative anomaly in the Terra Sirenum region. The outer ring of
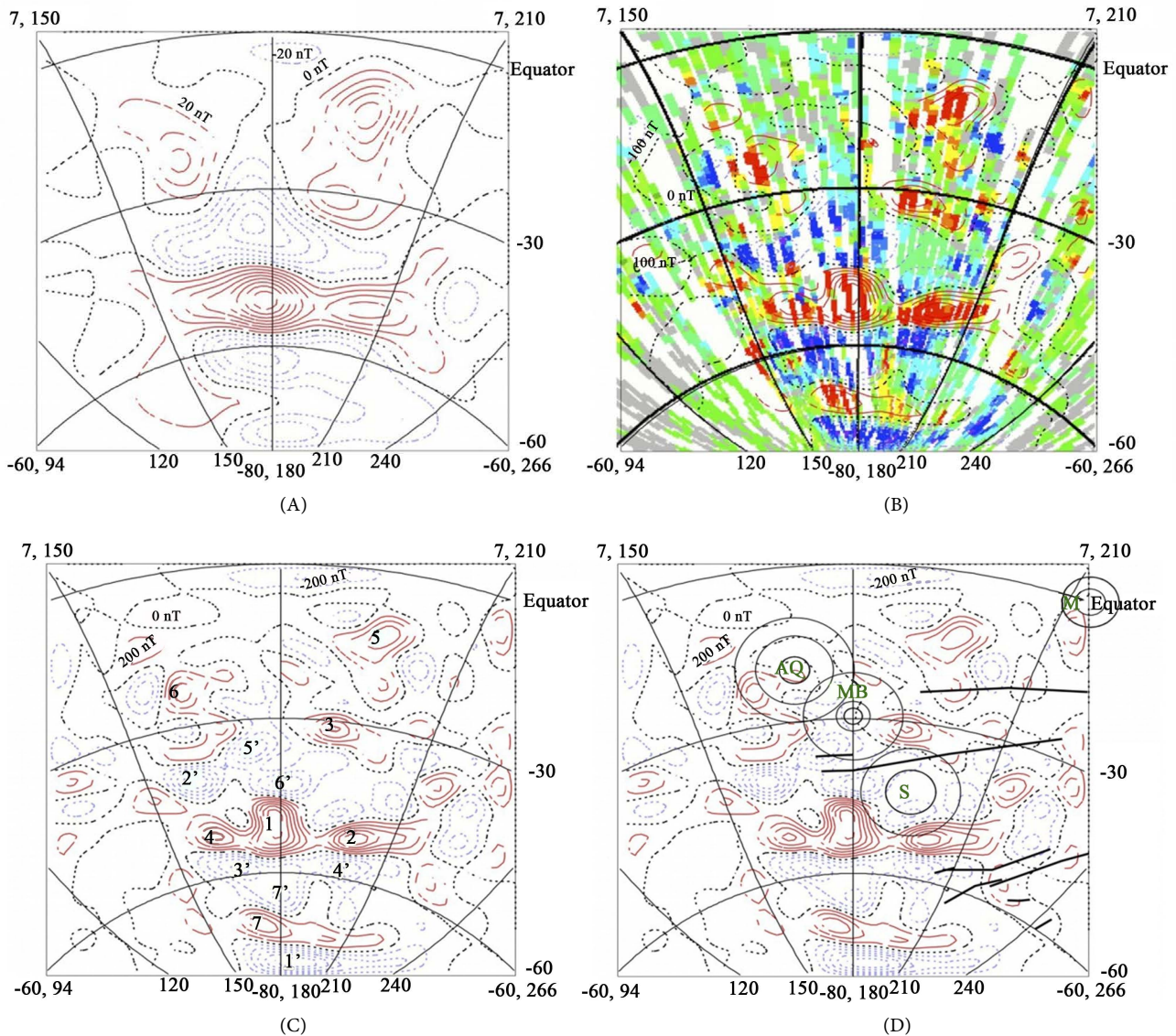
Figure 2. Magnetization in Terra Sirenum. Each base map uses MGS MAG Br data. (A) Data collected at 400 km (mapping) altitude (contour interval is 20 nT); (B) 400 km data downward continued to 100 km (contour interval is 100 nT) and correlated with aerobraking data (swaths) collected at the same altitude. Dark red represent strongly positive while dark blue represents strongly negative; (C) 400 km data downward continued to the surface (contour interval 200 nT). The numbers correspond to depth estimates; (D) Surface magnetization (contour interval 200 nT) with mapped faults [14] [15] and mapped regional multi-ringed basins [49] [50] (AQ = Al Qahira, MB = Memnonia-B, S = Sirenum, M = Mangala).

the Memnonia-B basin overlaps the third strongest of the positive and the fifth strongest of the negative anomalies, while the Al Qahira basin overlaps with the sixth strongest positive anomaly.

4.2. Regional Comparison

The magnetization in the Terra Meridiani region displays a number of similarities with the Terra Sirenum region. A small number of positive and negative sources have been selected based on the strongest radial fields for both regions. As expected, the magnitude of magnetization in Terra Meridiani is considerably

lower than that in Terra Sirenum. The amplitude of the Terra Meridiani magnetization for the strongest positive and strongest negative measures less than one-quarter of that in the Southern Hemisphere. However, for both regions the strongest positive source exceeds the strongest negative source by 40% with the ratio of the strongest positive to strongest negative sources matching within 2%.

5. Analysis

The pattern and characteristics of surface magnetization of the Terra Meridiani and Terra Sirenum regions may hold some clues on the timing, mechanism, and depth of Mars' magnetization. We attempt to infer the depth of magnetization from the characteristics of the field in the Terra Meridiani region and compare with that of Terra Sirenum, the site of Mars' strongest magnetization. Here, we use downward continuation to examine the decay for the strongest sources and the observed pattern of the surface magnetization to infer the depth of magnetization for Terra Meridiani and Terra Sirenum.

5.1. Decay with Altitude

We estimated magnetic source depth by analyzing how the crustal magnetization decays with altitude. First, we assume the sources act as radially oriented monopoles (*i.e.*, dikes) and can be represented by $Bz = q/r^2$ where q is source strength and r is distance from the source (altitude relative to the Martian surface). Because the magnitude of the sources increases rapidly with decreasing altitude, we plot the reciprocals of the square root of the radial field component against the altitude relative to the Martian surface (**Figure 3**). This establishes the depth at which the reciprocal reaches zero (*i.e.*, infinite magnitude), inferred as the depth to the top of the magnetic source. Two "best fits" were attempted with the data: Linear (directly above the source) and Parabolic (off-center from source). However, trying to fit the entire parabolic curve to the data resulted in larger error, so only a linear fit was used.

A total of ten (five positive and five negative) magnetic sources were selected for the Terra Meridiani region. The five positive sources range in magnitude from 100 - 300 nT, while the negative ones are slightly lower. The larger Terra Meridiani sources (1 - 4 and 1' - 4') can be extrapolated below the surface (**Figure 3(A)**), generally to a depth of 80 ± 20 km but with a range of ~30 - 160 km. However, source 5 displays a different behavior, with its reciprocal reaching zero just above the surface. This anomalous source may be the result of dimensions not well represented by this method or a surface anomaly different from others. For this region, positive and negative sources display no apparent difference in extrapolation.

Seven positive and seven negative sources were chosen for Terra Sirenum. The strongest positive source has a value of 1368 nT at the surface, corresponding to 175 nT located at 400 km, and the strongest negative source has a value of −812 nT at the surface and −67 nT at 400 km. Depths for the 14 (seven positive and seven negative) strongest sources are 65 ± 25 km (**Figure 3(B)**) and range from

(A)

(B)
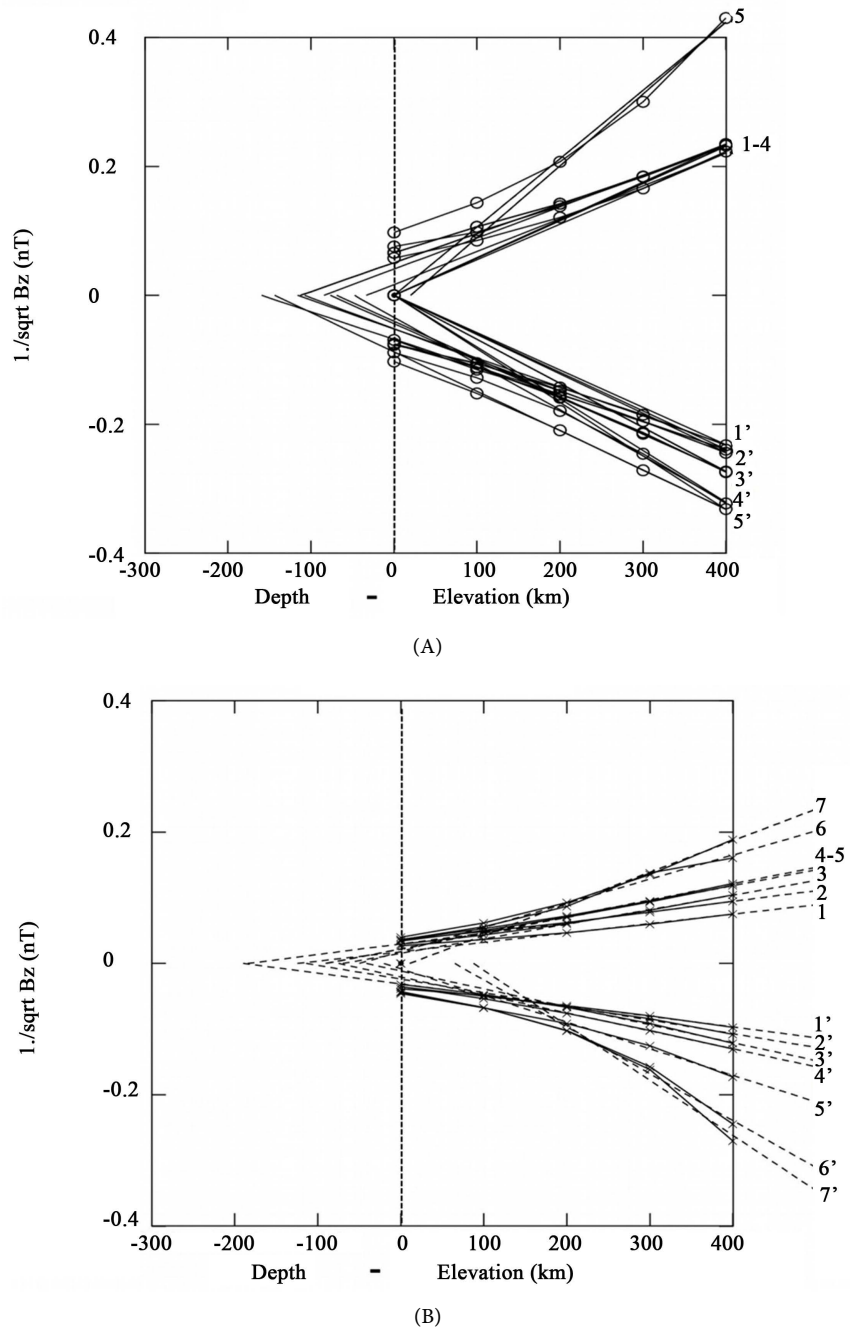
Figure 3. Decay with altitude for radially oriented monopole sources in (A) Terra Meridiani and (B) Southern Sirenum. The vertical dashed line represents the surface. Numbers represent sources from **Figure 1(C)** or Terra Meridiani and **Figure 2(C)** for Terra Sirenum. Depths range from ~35 - 160 km in Terra Meridiani and ~40 - 195 km in Terra Sirenum.

~20 - 190 km. Using a linear extrapolation, the positive and negative sources give about the same depths. The weakest negative sources, 6' and 7', are not well defined on the surface magnetization map (**Figure 2(C)**) and do not extrapolate beneath the surface. These sources have a weak signal and are thus swamped by noise, so they are not well represented as monopoles.
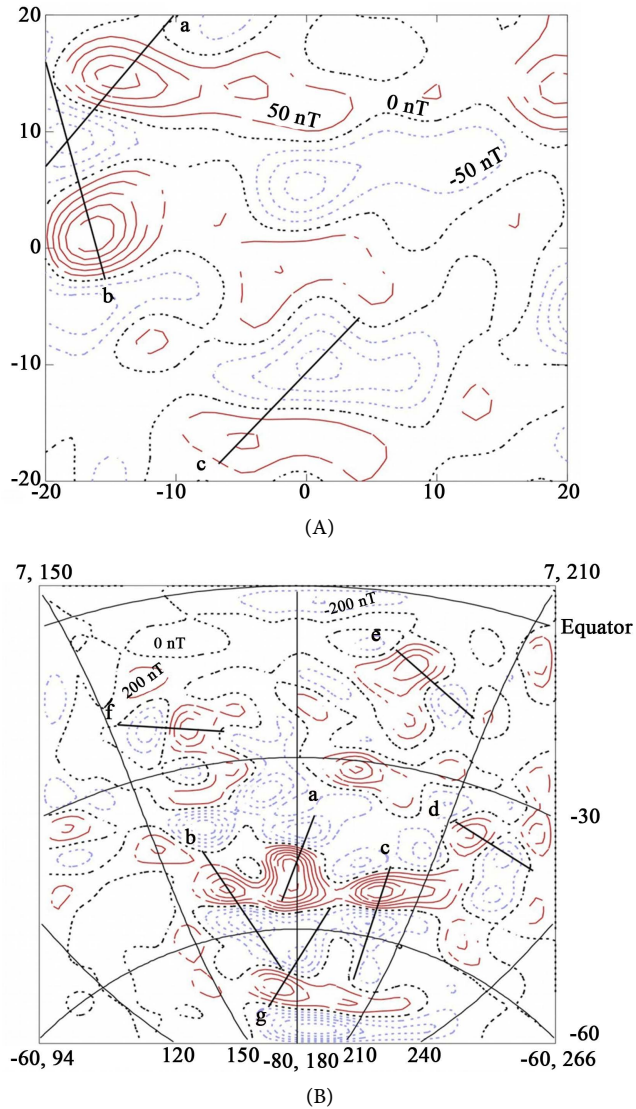
5.2. Peters' Method

Peters' Method of magnetic depth estimation for isolated sources was developed for Earth-based magnetic surveys and mining applications and works best for high latitudes (where the change in magnetic intensity in the horizontal direction can be taken as zero, resulting in a symmetrical anomaly), but produces good first-order approximations for other latitudes [48] [52]. The source of the magnetic anomaly is assumed to be two-dimensional with vertical sides, uniform and roughly vertical magnetization, and considerable depth extent. Using a contour map, the horizontal distance over which the contours of the magnetic (or gravity) anomaly are roughly equally spaced (a linear function of distance) is comparable to the source depth. Using a magnetic profile, draw two parallel lines with slopes equal to half the maximum gradient of the anomaly: One of the lines is tangent to the anomaly peak (point of inflection) and the other tangent to the anomaly minimum (point of inflection) (Figure 4). The horizontal distance x between these two lines is used to estimate the depth (d) to the top of the source: $x = 1.2d$ for a very thin body, $x = 1.6d$ for a body of intermediate thickness, and $x = 2d$ for a very thick body.

We generated magnetic profiles and applied Peters' Method to possible sources with equally spaced contours where inflection points could be determined (Figure 5). For Terra Meridiani, we chose three possible sources and estimate depths from 125 km for thick sources to 291 km for thin sources (Table 2). Possible sources in Terra Sirenum are more numerous and shallower, ranging from 82 km for thick sources to 234 km for thin sources (Table 2). Some of
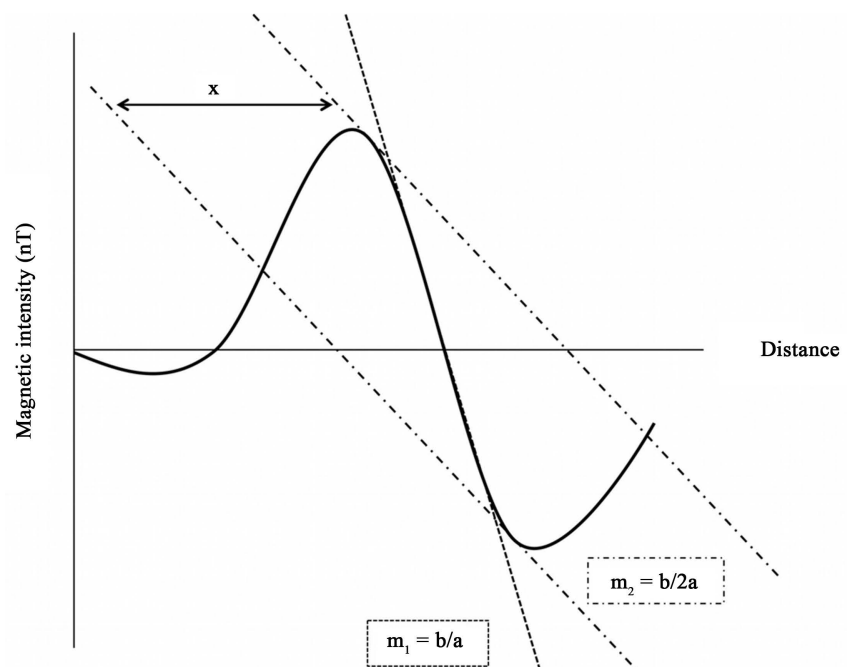
Figure 4. Illustration of Peters' method for an isolated magnetic anomaly, where m_1 is the slope of the maximum gradient (dashed line) and m_2 is the slope of half the maximum gradient (dot- dashed lines). The horizontal distance, x, between the dot-dashed lines is used to approximate the depth to the magnetic source (after [48]).

(A)

(B)

Figure 5. Source profiles chosen in (A) Terra Meridiani and (B) Southern Sirenum for Peters' method [52]. Maps are downward continued surface magnetization from **Figure 1(C)** and **Figure 2(C)**.

Table 2. Magnetic profiles and corresponding depths (in km) for potential sources (thick, intermediate, and thin) using Peters' method in Terra Meridiani and Terra Sirenum.

	a	b	c	d	e	f	g
Terra Meridiani							
thick	125	175	132				
intermediate	156	219	164				
thin	208	291	219				
Terra Cimmeria							
thick	121	95	140	129	111	99	82
intermediate	151	119	175	162	139	124	103
thin	201	158	234	216	185	164	137

these values do exceed estimates from previous workers (c.f. Section 2.3), but the thick to intermediate estimates are still feasible considering a lower (~20 mW/m^2) Martian heat flux at ~4 Ga (believed to be when the core dynamo shut down) allowing for magnetite, hematite, and/or pyrrhotite (although limited) as magnetic carriers.

The major parameters affecting magnetic source depth are found to be (1) initial mantle temperature, (2) mantle viscosity, and (3) the total radioactive content of Mars, which all affect heat flow [53]. By varying these parameters, crustal magnetization depths comparable to our depth estimates from both methods can be obtained. Without further constraints on these parameters, our estimates remain plausible.

5.3. Pressure Effects

As our depth estimates are considerably deeper than most other estimates, we consider the effects of pressure (from impacts and lithostatic) on magnetization. Due to the age of the Martian crust and prevalence of large craters, the upper 10 - 20 km of the crust has been inferred to be largely impact demagnetized [53]. That partial demagnetization occurs out to 1.4 basin radii for giant impact basins [5], but these effects vary with depth [54]. A number of our sources lie along outer rings of large impact basins and are close to or within the 1.4 basin radii demagnetization zone, indicating that high coercivity rocks (containing minerals such as single domain magnetite or multi-domain hematite) carry at least part of the remanent magnetization.

Laboratory experiments on pressure demagnetization have been carried out for samples of magnetite, titanomagnetite, hematite, titanohematite, and pyrrhotite [55]. While all samples significantly demagnetize at pressures ≥ few GPa, substantial variability exists in the data so that no demagnetization trend can be extracted. The effects of lithostatic pressure are of little concern because depths of ~100 km experience only about 1 GPa [56].

6. Future Missions to Mars

We have attempted to assess the depth of magnetization from the characteristics of the surface field. However, without knowing the detailed geometry of the magnetized region as well as the magnetization direction and the magnetic properties of the magnetized region, it is not possible to unambiguously establish the depth and extent of the sources. Mars' interior and its evolution remain largely unknown. More than 40 years have passed since the Viking Landers, the first successful landers on Mars, operated with seismometers. Viking Lander 2 touched down at Utopia Planitia on September 3, 1976. Both Landers transmitted images of the surface, took surface samples and analyzed them for composition and signs of life, studied atmospheric composition and meteorology, and delivered seismometers, unfortunately mounted on the landers' legs. The Viking 1 Lander seismometer, trapped in its unopened cage, could not function, but the Viking Lander 2 seismometer did record seismic activity, perhaps atmospheric,

before it ended communication on April 11, 1980 [57]. To this day, no seismometer has been placed on the Martian surface. A seismic network—possible with future additional seismometer placement—would provide invaluable information about Martian tectonic activity as well as the surface and interior structure of Mars.

The upcoming InSight (INterior Exploration using Seismic Investigations, Geodesy, and Heat Transport) mission to Mars will be the first dedicated to study the Martian interior. Rescheduled from a 2016 launch window due to a seismometer vacuum failure, the mission is now scheduled for launch in 2018. It will land in the Elysium Planitia with a 3-component broadband and short period seismometer, a heat flow probe, and a magnetometer to monitor the local magnetic field (atmospheric and as well as crustal). Seismic detection of Martian quakes or impacts offers the potential for determining the crustal and mantle structure. It could also establish the presence and state of the core and determine whether it's completely solid or still partially liquid [58]. A solidified core has been inferred on the basis of the current absence of a field suggesting the core no longer convects [3]. The InSight mission's planned measurements of heat flow will establish the current temperature with depth, giving the maximum depth of magnetization for the presence for a specified magnetic mineral. Many missions to Mars have returned numerous surprises, and InSight could answer many lingering questions about tectonics on Mars. How large is the core? Is it completely solid? How thick is the crust? How much heat flow still radiates from its interior? Answers to any of these questions will provide valuable constraints on Mars' magnetization and important information for understanding the magnetic field.

7. Conclusions

Surface magnetization maps of Terra Meridiani and Terra Sirenum are generated from MGS Magnetometer data acquired at 400 km altitude. This data, downward continued to lower altitudes, generally agrees with aerobraking data collected at corresponding altitudes, but aerobraking data is stronger. Outer rings of several large impact basins in both Terra Meridiani and Terra Cimmeria overlap with strong magnetic anomalies.

For both Terra Meridiani and Terra Sirenum, the amplitudes of positive anomalies exceed negative ones by about 40%. Also, aerobraking measurements in both regions showed this discrepancy. This ratio of the strongest positive to strongest negative sources for each region differs by only 2%. Perhaps stronger positive anomalies represent a fundamental characteristic of the Martian core dynamo. If so, then analyses of other regions should confirm the same effect.

We take two different approaches of determining depth to magnetization that yield source depths within the range estimated by most other authors. By examining the magnetization decay with downward continued altitude, we found depths generally between 80 ± 20 km in Terra Meridiani and 65 ± 25 km in Terra Sirenum. Peters' Method generates magnetic depths ranging from 125 km to 291 km in Terra Meridiani and 82 km to 234 km in Terra Sirenum depending on

the thickness of the source. If Martian heat flux at ~4 Ga was on the lower end ($\leq$~20 mW/m^2) [41] [44] [45], then our magnetic depths agree well with magnetite, hematite, and/or pyrrhotite as magnetic carriers. Furthermore, the lack of correlation between magnetization and other data or surface features further suggests deep sources.

Small regions of intense magnetization in Terra Meridiani resemble those in the Southern Hemisphere region of strongest magnetization, but have lower magnitude. Sources in both regions display similar decay with altitude when downward continued into the subsurface. These observations, combined with the source depths determined, do not confirm Martian magnetization as being the consequence of a process of surface spreading associated with ancient plate tectonics in the presence of a magnetic field. However, our analysis does not rule out the possibility of magnetic stripes and field reversals on Mars.

Acknowledgements

References

[1] Acuña, M.H., Connerney, J.E.P., Ness, N.F., Lin, R.P., Mitchell, D., Carlson, C.W., McFadden, J., Anderson, K.A., Rème, H., Mazelle, C., Vignes, D., Wasilewski, P. and Cloutier, P. (1999) *Science*, **284**, 790-793. https://doi.org/10.1126/science.284.5415.790

[2] Albee, A.L., Arvidson, R.E., Palluconi, F. and Thorpe, T. (2001) *Journal of Geophysical Research*, **106**, 23291-23316. https://doi.org/10.1029/2000JE001306

[3] Connerney, J.E.P., Acuña, M.H., Ness, N.F., Kletetschka, G., Mitchell, D.L., Lin, R.P. and Rème, H. (2005) *Proceedings of the National Academy of Sciences of the United States of America*, **102**, 14970-14975. https://doi.org/10.1073/pnas.0507469102

[4] Hood, L.L., Richmond, N.C., Pierazzo, E. and Rochette, P. (2003) *Geophysical Research Letters*, **30**, 1281. https://doi.org/10.1029/2002GL016657

[5] Mohit, P.S. and Arkani-Hamed, J. (2004) *Icarus*, **168**, 305-317.

[6] Lillis, R.J., Frey, H.V. and Manga, M. (2008) *Geophysical Research Letters*, **35**, L14203. https://doi.org/10.1029/2008GL034338

[7] Lillis, R.J., Frey, H.V., Manga, M., Mitchell, D.L., Lin, R.P., Acuña, M.H. and Bougher, S.W. (2008) *Icarus*, **194**, 575-596.

[8] Weiss, B.P., Vali, H., Baudenbacher, F.J., Kirschvink, J.L., Stewart, S.T. and Shuster, D.L. (2002) *Earth and Planetary Science Letters*, **201**, 449-463.

[9] Antretter, M., Fuller, M., Scott, E., Jackson, M., Moskowitz, B. and Solheid, P. (2003) *Journal of Geophysical Research*, **108**, 5049. https://doi.org/10.1029/2002je001979

[10] Stevenson, D.J. (2001) *Nature*, **412**, 214-219. https://doi.org/10.1038/35084155

[11] Arkani-Hamed, J. and Ghods, A. (2011) *Icarus*, **212**, 920-934.

[12] Mitchell, D.L., Lillis, R.J., Lin, R.P., Connerney, J.E.P. and Acuña, M.H. (2007) *Journal of Geophysical Research*, **112**, E01002. https://doi.org/10.1029/2005je002564

[13] Jurdy, D.M. and Stefanick, M. (2009) *Icarus*, **203**, 38-46.

[14] Scott, D.H. and Tanaka, K.L. (1986) Geologic Map of the Western Equatorial Region of Mars. United States Geological Survey Miscellaneous Investigations Series, Scale 1:15,000,000.

[15] Greeley, R. and Guest, J.E. (1987) Geologic Map of the Eastern Equatorial Region of Mars. United States Geological Survey Miscellaneous Investigations Series, Scale 1:15,000,000.

[16] Tanaka, K.L., Skinner Jr., J.A., Dohm, J.M., Irwin III, R.P., Kolb, E.J., Fortezzo, C.M., Platz, T., Michael, G.G. and Hare, T.M. (2014) Geologic Map of Mars. United States Geological Survey Scientific Investigations, Map 3292, Scale 1:20,000,000. https://doi.org/10.3133/sim3292

[17] Bandfield, J.L. (2002) *Journal of Geophysical Research*, **107**, 5042. https://doi.org/10.1029/2001je001510

[18] McLennan, S.M., Bell III, J.F., Calvin, W.M., Christensen, P.R., Clark, B.C., de Souza, P.A., Farmer, J., Farrand, W.H., Fike, D.A., Gellert, R., Ghosh, A., Glotch, T.D., Grotzinger, J.P., Hahn, B., Herkenhoff, K.E., Hurowitz, J.A., Johnson, J.R., Johnson, S.S., Jolliff, B., Klingelhöfer, G., Knoll, A.H., Learner, Z., Malin, M.C., McSween Jr., H.Y., Pocock, J., Ruff, S.W., Soderblom, L.A., Squyres, S.W., Tosca, N.J., Watters, W.A., Wyatt, M.B. and Yen, A. (2005) *Earth and Planetary Science Letters*, **240**, 95-121.

[19] Squyres, S.W. and Knoll, A.H. (2005) *Earth and Planetary Science Letters*, **240**, 1-10.

[20] Squyres, S.W., Knoll, A.H., Arvidson, R.E., Clark, B.C., Grotzinger, J.P., Jolliff, B.L., McLennan, S.M., Tosca, N., Bell, J.F., Calvin, W.M., Farrand, W.H., Glotch, T.D., Golombek, M.P., Herkenhoff, K.E., Johnson, J.R., Klingelhöfer, G., McSween, H.Y. and Yen, A.S. (2006) *Science*, **313**, 1403-1407. https://doi.org/10.1126/science.1130890

[21] Carr, M.H. and Head, J.W. (2010) *Earth and Planetary Science Letters*, **294**, 185-203.

[22] Espley, J.R. and Connerney, J.E.P. (2013) Crustal Magnetic Fields at Mars: Improved Interpretation through Higher Resolution. 44*th Lunar and Planetary Science Conference*, Abstract 2891.

[23] Sleep, N.H. (1994) *Journal of Geophysical Research*, **99**, 5639-5655. https://doi.org/10.1029/94JE00216

[24] Connerney, J.E.P., Acuña, M.H., Wasilewski, P.J., Ness, N.F., Rème, H., Mazelle, C., Vignes, D., Lin, R.P., Mitchell, D.L. and Cloutier, P.A. (1999) *Science*, **284**, 794-798. https://doi.org/10.1126/science.284.5415.794

[25] Nimmo, F. (2000) *Geology*, **28**, 391-394. https://doi.org/10.1130/0091-7613(2000)28<391:DIAAPC>2.0.CO;2

[26] Jurdy, D.M. and Stefanick, M. (2004) *Journal of Geophysical Research*, **109**, E10005. https://doi.org/10.1029/2004JE002277

[27] Purucker, M., Ravat, D., Frey, H., Voorhies, C., Sabaka, T. and Acuña, M. (2000) *Geophysical Research Letters*, **27**, 2449-2452. https://doi.org/10.1029/2000GL000072

[28] Zuber, M.T., Solomon, S.C., Phillips, R.J., Smith, D.E., Tyler, G.L. Aharonson, O., Balmino, G., Banerdt, W.B., Head, J.W., Johnson, C.L., Lemoine, F.G., McGovern, P.J., Neumann, G.A., Rowlands, D.D. and Zhong, S. (2000) *Science*, **287**, 1788-1793. https://doi.org/10.1126/science.287.5459.1788

[29] Nimmo, F. and Gilmore, M.S. (2001) *Journal of Geophysical Research*, **106**, 12315-12323. https://doi.org/10.1029/2000JE001325

[30] Voorhies, C.V., Sabaka, T.J. and Purucker, M. (2002) *Journal of Geophysical Research*, **107**, 5034. https://doi.org/10.1029/2001je001534

[31] Parker, R.L. (2003) *Journal of Geophysical Research*, **108**, 5006. https://doi.org/10.1029/2001je001760

[32] Langlais, B., Purucker, M.E. and Mandea, M. (2004) *Journal of Geophysical Research*, **109**, E02008. https://doi.org/10.1029/2003je002048

[33] Dunlop, D.J. and Arkani-Hamed, J. (2005) *Journal of Geophysical Research*, **110**, E12S04. https://doi.org/10.1029/2005je002404

[34] Hood, L.L., Harrison, K.P., Langlais, B., Lillis, R.J., Poulet, F. and Williams, D.A. (2010) *Icarus*, **208**, 118-131.

[35] Rochette, P., Lorand, J.-P., Fillion, G. and Sautter, V. (2001) *Earth and Planetary Science Letters*, **190**, 1-12.

[36] Kletetschka, G., Wasilewski, P.J. and Taylor, P.T. (2000) *Meteoritics & Planetary Science*, **35**, 895-899. https://doi.org/10.1111/j.1945-5100.2000.tb01478.x

[37] Christensen, P.R., Bandfield, J.L., Clark, R.N., Edgett, K.S., Hamilton, V.E., Hoefen, T., Kieffer, H.H., Kuzmin, R.O., Lane, M.D., Malin, M.C., Morris, R.V., Pearl, J.C., Pearson, R., Roush, T.L., Ruff, S.W. and Smith, M.D. (2000) *Journal of Geophysical Research*, **105**, 9623-9642. https://doi.org/10.1029/1999JE001093

[38] Christensen, P.R., Morris, R.V., Lane, M.D., Bandfield, J.L. and Malin, M.C. (2001) *Journal of Geophysical Research*, **106**, 23873-23885. https://doi.org/10.1029/2000JE001415

[39] Arvidson, R.E., Poulet, F., Morris, R.V., Bibring, J.-P., Bell III, J.F., Squyres, S.W., Christensen, P.R., Bellucci, G., Gondet, B., Ehlmann, B.L., Farrand, W.H., Fergason, R.L., Golombek, M., Grifffes, J.L., Grotzinger, J., Guinness, E.A., Herkenhoff, K.E., Johnson, J.R., Klingelhofer, G., Langevin, Y., Ming, D., Seelos, K., Sullivan, R.J., Ward, J.G., Wiseman, S.M. and Wolff, M. (2006) *Journal of Geophysical Research*, **111**, E12S08. https://doi.org/10.1029/2006je002728

[40] Goetz, W., Leer, K., Gunnlaugsson, H.P., Bartlett, P., Basso, B., Bell, J., Bertelsen, P., Binau, C.S., Chu, P.C., Gorevan, S., Hansen, M.F., Hviid, S.F., Kinch, K.M., Klingelhöfer, G., Kusack, A., Madsen, M.B., Ming, D.W., Morris, R.V., Mumm, E., Myrick, T., Olsen, M., Ming, D.W., Morris, R.V., Mumm, E., Myrick, T., Olsen, M., Squyres, S.W., Wilson, J. and Yen, A. (2008) *Journal of Geophysical Research*, **113**, E05S90. https://doi.org/10.1029/2006je002819

[41] Davies, G.F. and Arvidson, R.E. (1981) *Icarus*, **45**, 339-346.

[42] Hauck, S.A. and Phillips, R.J. (2002) *Journal of Geophysical Research*, **107**, 5052. https://doi.org/10.1029/2001je001801

[43] McKenzie, D., Barnett, D.N. and Yuan, D.-N. (2002) *Earth and Planetary Science Letters*, **195**, 1-16.

[44] McGovern, P.J., Solomon, S.C., Smith, D.E., Zuber, M.T., Simons, M., Wieczorek, M.A., Phillips, R.J., Neumann, G.A., Aharonson, O. and Head, J.W. (2004) *Journal of Geophysical Research*, **109**, E07007. https://doi.org/10.1029/2004je002286

[45] Grott, M., Hauber, E., Werner, S.C., Kronberg, P. and Neukum, G. (2007) *Icarus*, **186**, 517-526.

[46] Merrill, R.T., McElhinny, M.W. and McFadden, P.L. (1998) The Magnetic Field of the Earth. Academic Press, San Diego, 539 p.

[47] Nagy, A.F., Winterhalter, D., Sauer, K., Cravens, T.E., Brecht, S., Mazelle, C., Crider, D., Kallio, E., Zakharov, A., Dubinin, E., Verigin, M., Kotova, G., Axford, W.I., Bertucci, C. and Trotignon, J.G. (2004) *Space Science Reviews*, **111**, 33-114. https://doi.org/10.1023/B:SPAC.0000032718.47512.92

[48] Blakely, R.J. (1996) Potential Theory in Gravity and Magnetic Applications. Cambridge University Press, Cambridge, 464 p.

[49] Schultz, P.H., Schultz, R.A. and Rogers, J. (1982) *Journal of Geophysical Research*, **87**, 9803-9820. https://doi.org/10.1029/JB087iB12p09803

[50] Schultz, R.A. and Frey, H.V. (1990) *Journal of Geophysical Research*, **95**, 14175-14189. https://doi.org/10.1029/JB095iB09p14175

[51] Frey, H. (2008) *Geophysical Research Letters*, **35**, L13203. https://doi.org/10.1029/2008gl033515

[52] Peters, L.J. (1949) *Geophysics*, **14**, 290-320. https://doi.org/10.1190/1.1437537

[53] Arkani-Hamed, J. (2005) *Journal of Geophysical Research*, **110**, E08005. https://doi.org/10.1029/2004je002397

[54] Kletetschka, G., Connerney, J.E.P., Ness, N.F. and Acuña, M.H. (2004) *Meteoritics and Planetary Science*, **39**, 1839-1848. https://doi.org/10.1111/j.1945-5100.2004.tb00079.x

[55] Louzada, K.L., Stewart, S.T., Weiss, B.P., Gattacceca, J., Lillis, R.J. and Halekas, J.S. (2011) *Earth and Planetary Science Letters*, **305**, 257-269.

[56] Louzada, K.L., Stewart, S.T., Weiss, B.P., Gattacceca, J. and Bezaeva, N.S. (2010) *Earth and Planetary Science Letters*, **290**, 90-101.

[57] Anderson, *et al.* (1977) *Journal of Geophysical Research*, **82**, 4524-4546. https://doi.org/10.1029/JS082i028p04524

[58] Khan, A., van Driela, M., Bose, M., Giardini, D., Ceylan, S., Yan, J., Clinton, J., Buchner, F., Lognonne, P., Murdoch, N., Mimoun, D., Panning, M., Knapmeyer, M. and Banerdt, W.B. (2016) *Physics of the Earth and Planetary Interiors*, **258**, 28-42.